Rebound dynamics of two droplets simultaneously impacting a flat superhydrophobic surface

Xin Wang[1], Dian-Ji Lin[1], Yi-Bo Wang[1], Shu-Rong Gao[1], Yan-Ru Yang[1], and Xiao-Dong Wang[1]

[1]North China Electric Power University

May 5, 2020

Abstract

In this letter, we investigate the rebound dynamics of two equally sized droplets simultaneously impacting a superhydrophobic surface via lattice Boltzmann method (LBM) simulations. We discover three rebound regimes depending on the droplet distance: a complete-coalescence-rebound (CCR) regime, a partial-coalescence-rebound (PCR) regime, and a no-coalescence-rebound (NCR) regime. We demonstrate that the rebound regime is closely associated with dynamic behaviors of the formed liquid ridge or bridge between two droplets. We also present the contact time in the three regimes. Intriguingly, although partial coalescence takes places, the contact time is still dramatically shortened in the PCR regime, which is even smaller than that of a single droplet impact. These findings provide new insights into the contact time of multiple droplets impact, and thereby offering useful guidance for some application such as anti-icing, self-cleaning, and so forth.

When a droplet impacts a superhydrophobic surface, it undergoes spreading and retraction, and eventually bounces off the surface.[1] The contact time, t_c, defined as a length of time interval for the droplet remaining in contact with the solid surface, is a very important parameter to measure the surface superhydrophobicity. A short contact time is in particular favorable to serval applications, i.e. self-cleaning,[1,2] anti-corrosion,[3]anti-icing.[4,5] On the contrary, a long contact time is the most basic requirement for spray cooling.[6]

It has been widely recognized that, for low-viscosity fluids such as water, the rebound dynamics on superhydrophobic surfaces is dominated by inertial and capillary forces, so that the contact time depends only on the Weber number, following a relation$t_c \, (D_0/V_0) f \, (We)$,[7,8]here$We = \rho{}_0{}^2 D_0/\sigma$with ρ, D_0, V_0, andσ being the liquid density, droplet diameter, impact velocity, and liquid surface tension, respectively. In a low impact velocity region with $We<1$, the impacting droplet can be treated as an elastic ball because of its small deformation. Since the deformation is described by a Hertz shock, the contact time scales as$t_c \, (D_0/V_0) We^{2/5}$, varying as$V_0^{-1/5}$.[8]However, when $We>1$, despite the deformation amplitude and details are found to depend strongly on the impact velocity, the contact time is independent of the impact velocity in a wide range of velocities. As a result, the contact time follows a scale$t_c \, (D_0/V_0)\mathrm{We}^{1/2}$.[8]The prefactor is usually determined to be 2.6 for a water droplet impacting superhydrophobic surfaces at$We>1$,[7,8] implying that there is a limit of the contact time. Many efforts have been devoted to proposing new methods to reduce the contact time, aiming at breaking the limit. For example, using superhydrophobic surfaces with a macroscale ridge to generate a non-axisymmetric retraction,[7,9-11]designing superhydrophobic surfaces with specific microstructures to induce a pancake bouncing,[12-15] and texturing superhydrophobic surfaces with a point-like superhydrophobic macrotexture[16] or using convex superhydrophobic surfaces[17] to trigger a ring-bouncing.

It should be emphasized that the previous studies[7-17]focused only on a single droplet impact; however, multiple droplets impact is more frequently encountered in practical applications. When multiple droplets impact simultaneously a superhydrophobic surfaces, they will coalesce with each other, forming a large droplet.

Because of complex interactions caused by coalescence, the rebuond dynamics may become extremely abstruse. Moreover, coalescence also inevitably gives rise to viscous dissipation even if on superhydrophobic surfaces.[18,19] As a result, the contact time should depend on both the Weber and Reynolds numbers and thereby increasing as compared to the single droplet impact. Unfortunately, how the coalescence influnces the rebound dyanmics and resultant contact time of the multiple droplets impact remians poorly understood. Recently, several studies[20,21] numerically studied impact behaviors of multiple droplets on hydrophilic and hydrophobic surfaces. These studies demonstrated that the droplet-to-droplet coalescence dynamics signifjcanlty alters spreading and retraction behaviors of the droplets, leading to significantly different outcomes from the single droplet impact.

In this letter, we ivestigate the reboud dynamics of two equally sized droplets simultaneously impacting a superhydrophobic surface via LBM simulations. We discover three rebound regimes depending on the distance between the two droplets: a CCR regime, a PCR regime, a NCR regime. We show that the liquid ridge or bridge formed between the two droplets plays different role in coalescence dynamcis in the three regimes. We also demonstrate that although partial coalescence takes places between the two droplets, the contact time is still dramatically shortened in the PCR regime, even smaller than that of the single droplet impact.

In this work, we employ a three-dimensional nineteen-velocity (D3Q19) Shan-Chen model incorporated with the multi-relaxation-time (MRT) collision operator, namely MRT pseudopotential lattice Boltzmann model (MRT-LBM), due to the fact that the MRT model overcomes the numerical instability and reduces spurious currents[22,23] (see the supplementary material S1 for Multi-relaxation-time pseudopotential lattice Boltzmann model). The schematic of two equally sized droplets simultaneously impacting a superhydrophobic surface is illustrated in**Fig. 1** . Dimensions of the computational box are$N_x \times N_y \times N_z$ =240×400×200 lattice units (lu). The box contains two kinds of immiscible fluids, liquid droplets and surrounding gas. The physical properties of the liquid and gas are listed in **Table 1** . The two side-by-side spherical droplets are placed just above the box bottom. They have the same diameter of D_0=60 lu and identical impact velocity of V_0 (lu ts^{-1}). The normalized distance between the two droplets is $L = l / D_0$, where $l$is the center-to-center distance between the two droplets. The box bottom is set as a flat superhydrophobic surface with a contact angle of$_0$=157°. No slip boundary conditions are imposed on the bottom and top of the box, whereas periodic boundary conditions are specified to the box side walls. Because the droplet diameter is far less than the capillary length,[24] the influence of gravity can be neglected. We validate the model by Laplace's law of a stationary droplet[21] as well as the contact time of a single droplet impacting a superhydrophobic surface.[10,14] (see the supplementary material S1 for model validation).

We start our simulations with a high Weber number of 35. By varying the distance L , we discover that after two droplets impact a flat superhydrophobic surface, they always bounce off the surface and exhibit three different rebound regimes depending on L : a CCR regime in a small L range, a PCR regime in a moderate L range, and a NCR regime in a large L range, as shown in **Figs.2-4** .

For the CCR regime, the two droplets completely coalesce before bouncing off the surface. **Figure 2(a)** illustrates the morphology evolution of the two droplets with a small L =1.17. After impacting the surface, the two droplets start to spread, forming rims in their perimeters. The rims of the two droplets intensely collide each other at the initial stage of spreading because of the small$L$. Subsequently, the colliding rims develops into a connecting ridge. The strong inertial force gives the rims large enough kinetic energy, which facilitates the fluid flowing in the ridge and makes the ridge move upwards, as shown at τ =0.48 in **Fig.2(b)** . Additionally, such an earlier collision also triggers the fluid flowing toward to the two ends of the ridge, as shown atτ =0.48 in **Fig. 2(c)** , resulting in the generation of two liquid lobes. Accompanied with continuous spreading, the ridge and liquid lobes rapidly grow until the two droplets reach the maximum spreading diameters. Meanwhile, two puddles and peripheral bulges form on the two sides of the ridge. After that, the two droplets start to retract due to the superhydrophobicity of the surface. According to the Young-Laplace equation, the puddles have concave interfaces and thereby have low pressures in the liquid phase. As a result, the liquid transports from the peripheral bulges and the ridge center to the puddles, as shown at τ =0.71 and 1.11 in**Figs. 2(b)** and **2(c)** , which makes the ridge height decrease, the two puddles shrink, and the two liquid lobes expand, and finally the two droplets coalesce into a cross-like morphology. Whereafter the cross-like droplet retracts mainly along two intersecting directions of the cross, i.e., the x and $y$directions, and the retraction in the y direction is faster than that in the x direction, forming an upright hump at the center of the cross. The hump height continuously increases with the retraction in the x and y directions. Therefore, the droplet gradually elongates in the vertical direction, i.e., the z direction, and its footprint gradually decreases with the retraction. As a consequence, the elongated droplet evolves into a parachute-shaped and finally bounces off the surface.

For the PCR regime, the two droplets partially coalesce before they bounce off the surface.**Figure 3(a)** shows the morphology evolution of the two droplets with a moderate$L$ =1.67. With such a value of L , the effect of inertial force becomes weaker when the rims of the two droplets touch each other, and hence, the touched rims possess less kinetic energy, which leads to the formation of a shorter ridge. Compared with the CCR regime, the length of the ridge is always less than the spreading diameter and no liquid lobes are generated on the two ends of the ridge, which significantly alter the coalescence dynamics. Two puddles and peripheral bulges are still generated in the spreading stage, which are similar to those in the CCR regime. Likewise, in the retraction stage, the liquid flows from the peripheral bulges and the ridge center into the puddles, as shown at τ =0.95 in **Figs. 3(b)** and**3(c)** . Accompanied with the shrinking of the puddles, the two ends of the ridge become flat and the height of the ridge decreases, and finally the ridge develops into a wider liquid bridge. After that, the further retraction makes the fluid flow upward, forming two uprising humps on the two sides of the bridge. In this period, because of the presence of the two humps, the retraction in the x direction is significantly stronger than that in the y direction, as shown atτ =1.43 in **Figs. 3(b)** and **3(c)** . Subsequently, the retraction in the y direction accelerates, so that the two humps continue to rise and get close to each other. The uprising humps pull the liquid bridge connecting them and makes the bridge depart from the surface, forming a two contact zones between the droplet and surface, as shown at τ =2.22 in **Figs.3(b)** and **3(c)** . When the two contact zones shrink to two points, the droplet evolves into a teeth-shaped and bounces off the surface.

For the NCR regime, the two droplets fail to coalesce before bouncing off the surface. **Figure 4(a)** presents the morphology evolution of the two droplets with a large L =2.00. After the two droplet impact the surface, they begin to spreads separately. With the large L , the rims touch each other in the later stage of spreading, and inertial force becomes therefore negligibly small. Because the touched rims have extremely low kinetic energy, a very short liquid bridge forms between the two droplets. Soon after the touch, the two droplets start to retract, so that the liquid bridge almost dose not grow up and no ridge is formed. Similar to the CCR and ICR regimes, two puddles generate on the two sides of the liquid bridge. In the retraction stage, the liquid flows from the peripheral bulges into the puddles, leading to the shrinking of the puddles, as shown atτ =0.95 in **Figs. 4(b)** and **4(c)** , and eventually two uprising humps form on the two sides of the bridge, as shown at τ =1.35 in **Figs** . **4(b)** and**4(c)** . It is worth noting that the liquid bridge is stretched in the y direction during the whole retraction. As the two humps continuously rise, the coalescing droplet is elongated into two columns and the liquid bridge gradually becomes thin, as shown at τ =2.22 shown in **Fig. 4(b)** and **4(c)** . Owing to the Rayleigh instability,[25] the liquid bridge ruptures, and hence, the coalescing droplet is split into the two elongated droplets. Finally, the two elongated droplets separately bounce off the surface.

Figure 5 shows the normalized contact time,τ_c, as a function of L at We =35. The dotted line in **Fig. 5** represents the contact time of a single droplet impacting a superhydrophobic surface, whose value is found to beτ_c=2.62 in our simulations. It can be seen that τ_c is closely dependent on L . The yellow zone denotes the CCR regime with small L . In this regime, the intense collision of rims generates a ridge with two growing lobes, making the two droplets coalesce completely before bouncing off the surface. The coalescence causes a large viscous dissipation and delays the rebounding, and thereby increasing the contact time. This effect becomes weaker at a larger L , so that the contact time declines with L in the CCR regime. The green zone denotes the PCR regime with moderate L . In this regime, because of the short ridge and no lobes forming on the two ends of the ridge, two uprising humps are generated in the retraction stage, which make the coalescing droplet form two contact zones with the surface, so that only partial coalescence takes places before bouncing off the surface. Intriguingly, the contact time in this regime remains almost at a constant value of τ_c=2.46, lower than that of a single droplet impact. The red zone denotes the NCR regime with large L . In this regime, a liquid bridge forms between the two droplets, instead of the formation of a ridge. The two droplet complete spreading and retraction nearly separately. However, the elongated liquid bridge links the two droplets and hinders their retraction, and hence, the contact time is slightly larger than that of a single droplet impact.

We further study the rebound dynamics of two droplets impacting a superhydrophobic surface at various Weber numbers. The rebound regimes and contact time are illustrated in **Fig. 6** . At two high We =20 and 35, three rebound regimes all take place, with the CCR regime in a small L range, the PCR regime in a moderate L range, and the NCR regime in a large L range. At a moderate We =10, the CCR and PCR regimes take place, whereas the NCR regime disappears. At two low We =1 and 5, only the CCR regime takes place. In the PCR regime, the contact time is smaller than or equal to that of a single droplet impact, regardless of the Weber number. In the NCR and CCR regimes, the contact time is larger than that of a single droplet impact. In particular, the contact time in the CCR regime is significantly larger than that of a single droplet impact and strongly depends on both We and L . As shown in the yellow zone in **Fig. 6** , at the moderate and high We =10, 20, and 35, the contact time declines with L , whereas an opposite tendency occurs at the low We =1 and 5. This difference arises from different coalescence and rebound dynamics. As shown in **Fig. 2** , at the moderate and high We , when two droplets come into contact with each other, rims have been formed in their periphery, so that intense collision of the rims dominates the coalescence and rebound dynamics. However, at the low We , when two droplets touch each other, they remain nearly spherical; therefore, a liquid bridge produces between the two droplets, and the bridge growth and impact dominates the coalescence and rebound dynamics, as shown in **Fig. S3** (see the supplementary material S2), which resembles coalescence-induced self-jumping of droplets on superhydrophobic surfaces.[19,27] Thus, a small L makes the liquid bridge impact the surface earlier, which promotes the droplet rebound and thereby reducing the contact time.

According to the above results, we speculate that the contact time in the CCR regime for two droplets impact should be longer when the surface wettability changes from superhydrophobic to hydrophobic. The rebound may fail on hydrophobic surfaces with high Weber numbers and small droplet distances. We add an extra simulation with ϑ_0=122°, We =35, and L =1. Because of the intense collision of rims, the formed ridge is extremely strongly elongated in the x direction, so that the coalescing droplet undergoes several times oscillation and eventually adhere to the surface. (see the supplementary material S3)

In conclusion, using MRT-LBM simulations, we investigate the rebound dynamics of two equally-sized droplets simultaneously impacting a flat superhydrophobic surface. Our emphasis is placed on revealing how the Weber number and droplet distance influence the contact time. We discover three rebound regimes at high Weber numbers depending on values of L : a CCR regime in a small L range, a PCR regime in a moderate L range, and a NCR regime in a large L range. When Weber numbers fall into the moderate or low range, the NCR regime or both the NCR and the PCR regime disappear. We demonstrate that the contact time is longer than that of a single droplet impact in the CCR and the NCR regime; however, intriguingly, it is less than that of a single droplet impact in the PCR regime. We discuss the impact dynamics in detail to understand the mechanism behind the three rebound regimes. We believe that our simulations provide useful information for practical applications such as self-cleaning, anti-corrosion, anti-icing, and so forth.

Acknowledgments

This study was partially supported by National Natural Science Foundation of China (No. 51936004), National Science Fund for Distinguished Young Scholars of China (No. 51525602), Science Fund for Creative Research Groups of the National Natural Science Foundation of China (No. 51821004), and Fundamental Research Funds for the Central Universities (No. 2017ZZD006).

References

1. X. Deng, L. Mammen, H. J. Butt, and D. Vollmer, Science 335, 67 (2012).
2. A. Tuteja, W. Choi, M. Ma, J. M. Mabry, S. A. Mazzella, G. C. Rutledge, G. H. McKinley, and R. E. Cohen, Science 318, 1618 (2007).
3. J. Ma, X. Y. Zhang, D. P. Wang, D. Q. Zhao, D. W. Ding, K. Liu, and W. H. Wang, Appl. Phys. Lett. 104, 173701 (2014).
4. L. Mishchenko, B. Hatton, V. Bahadur, J. A. Taylor, T. Krupenkin, and J. Aizenberg, ACS Nano 4, 7699 (2010).
5. S. Jung, M. K. Tiwari, N. V. Doan, and D. Poulikakos, Nat. Commun. 3, 615 (2010).
6. M. Visaria and I. Mudawar, Int. J. Heat Mass Transfer 51, 2398 (2008).
7. J. C. Bird, R. Dhiman, H. M. Kwon, and K. K. Varanasi, Nature 503, 385 (2013).
8. D. Richard, C. Clanet, and D. Quéré, Nature 417, 811 (2002).
9. K. Regulagadda, S. Bakshi, and S. K. Das, Phys. Fluids 29, 082104 (2017).
10. A. Gauthier, S. Symon, C. Clanet, and D. Quéré, Nat. Commun. 6, 8001 (2015).
11. D. J. Lin, L. Wang, X. D. Wang, and W. M. Yan, Int. J. Heat Mass Transfer 132, 1105 (2019).
12. Y. Liu, L. Moevius, X. Xu, T. Qian, J. M. Yeomans, and Z. Wang Nat. phys. 10, 515 (2014).
13. L. Moevius, Y. Liu, Z. Wang, and J. M. Yeomans, Langmuir 30, 13021 (2014).
14. A. M. Moqaddam, S. S. Chikatamarla, and I. V. Karlin, J. Fluid Mech. 824, 866 (2017).
15. J. Song, M. Gao, C. Zhao, Y. Lu, L. Huang, X. Liu, C. J. Carmalt, X. Deng, and I. P. Parkin, ACS Nano 11, 9259 (2017).
16. P. Chantelot, A. M.Moqaddam, A. Gauthier, S. S. Chikatamarla, C. Clanet, , I. V. Karlin, and D. Quéré, Soft Matter 14, 2227 (2018).
17. Y. Shen, S. Liu, C. Zhu, J. Tao, Z. Chen, H. Tao, L. Pan, G. Wang, and T. Wang, Appl. Phys. Lett. 110, 221601 (2017).
18. J. B. Boreyko, C. H. Chen, Phys. Rev. Lett. 103, 184501 (2009).
19. F. F. Xie, G. Lu, X. D. Wang, B. B. Wang, Langmuir 34, 2734 (2018).
20. K. Ashoke Raman, J. Colloid interface Sci. 516, 232 (2018).
21. X. Cheng, Y. Zhu, L. Zhang, D. Zhang, and T. Ku, Phys. Fluids 30, 042102 (2018).
22. D. Zhang, K. Papadikis, and S. Gu, Int. J. Multiphase Flow 64, 11 (2014).
23. Y. Shi, G. H. Tang, and H. H. Xia, Int. J. Heat Mass Transfer 88, 445 (2015).
24. X.D. Wang, Y. Zhang, D.J. Lee, and X.F. Peng, Langmuir 23, 9258 (2007).
25. L. Rayleigh, Proc. R. Soc. London 29, 71 (1879).
26. F.F. Xie, G. Lu, X.D. Wang, D.Q. Wang, Langmuir, 34, 11195 (2018).

Table and Figure Captions

Table 1 . Physical properties of droplet and gas.

FIG. 1 . Schematic of two equally sized droplets simultaneously impacting a flat superhydrophobic surface.

FIG. 2 . Complete-coalescence-rebound (CCR) regime. (a) Selected image sequence of impact and rebound behaviors of two droplets on a flat superhydrophobic surface with L =1.17 and We =35. The velocity fields are extracted along the mid y (b) and the mid$x$ (c) plane passing through the box. The normalized time is defined as$\tau = t\ /(\rho P\ {}_0{}^3/)^{1/2}$.

FIG. 3 . Partial-coalescence-rebound (PCR) regime. (a) Selected image sequence of impact and rebound behaviors of two droplets on a flat superhydrophobic surface with L =1.67 and We =35. The velocity fields are extracted along the mid y (b) and the mid$x$ (c) plane passing through the box. The normalized time is defined as$\tau = t\ /(\rho P\ {}_0{}^3/)^{1/2}$.

FIG. 4 . No-coalescence-rebound regime (NCR). (a) Selected image sequence of impact and rebound behaviors of two droplets on a flat superhydrophobic surface with L =2.00 and We =35. The velocity fields are extracted along the mid y (b) and the mid$x$ (c) plane passing through the box. The normalized time is defined as$\tau = t\ /(\rho P\ {}_0{}^3/)^{1/2}$.

FIG. 5 . The normalized contact time as a function of the droplet distance at We =35.

FIG. 6 . The normalized contact time as a function of the droplet distance at various Weber numbers.

Table 1 . Physical properties of droplet and gas.

Fluids	ρ (mu lu^{-3})	μ (lu^{2} ts^{-1})	(mu ts^{-2})
Droplet	0.455	7.58×10^{-3}	7.751×10^{-3}
Gas	6.06×10^{-4}	2.295×10^{-7}	

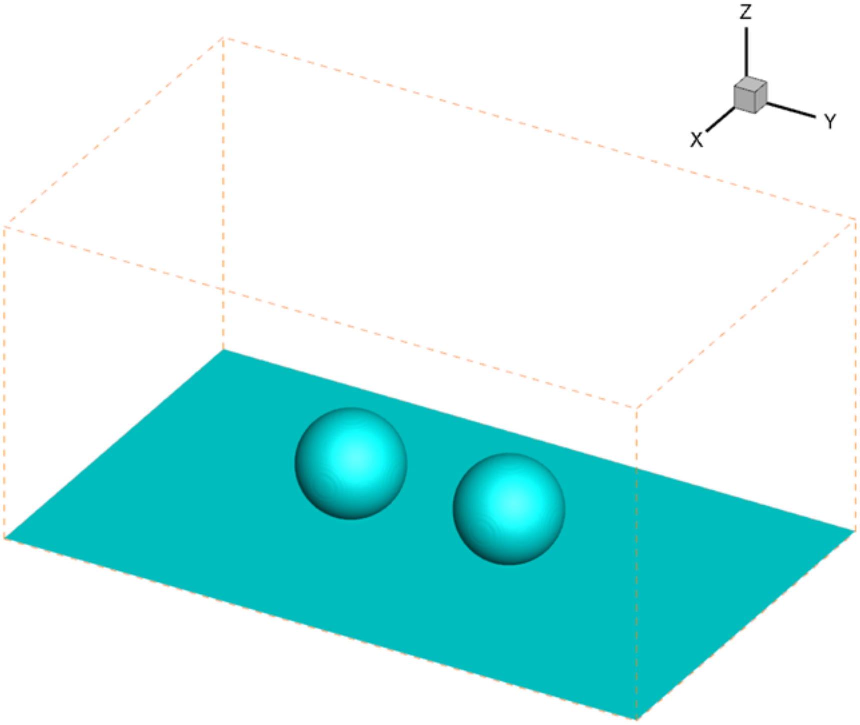

FIG. 1 . Schematic of two equally sized droplets simultaneously impacting a flat superhydrophobic surface.

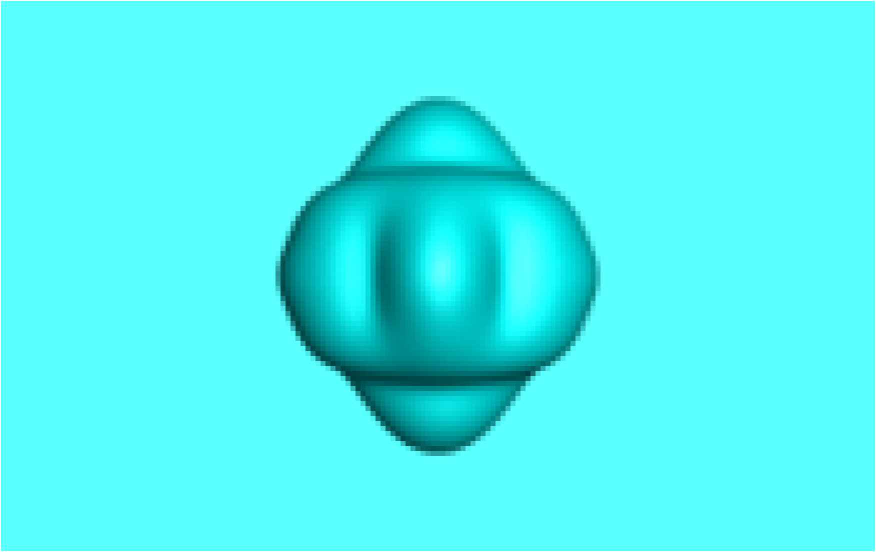

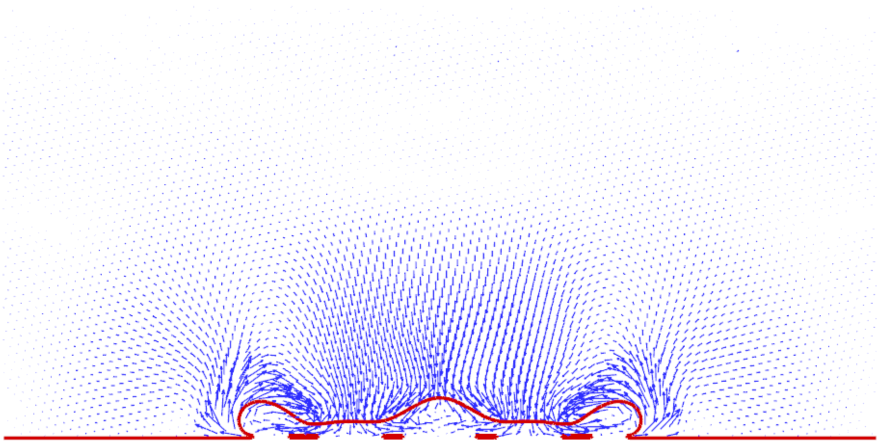

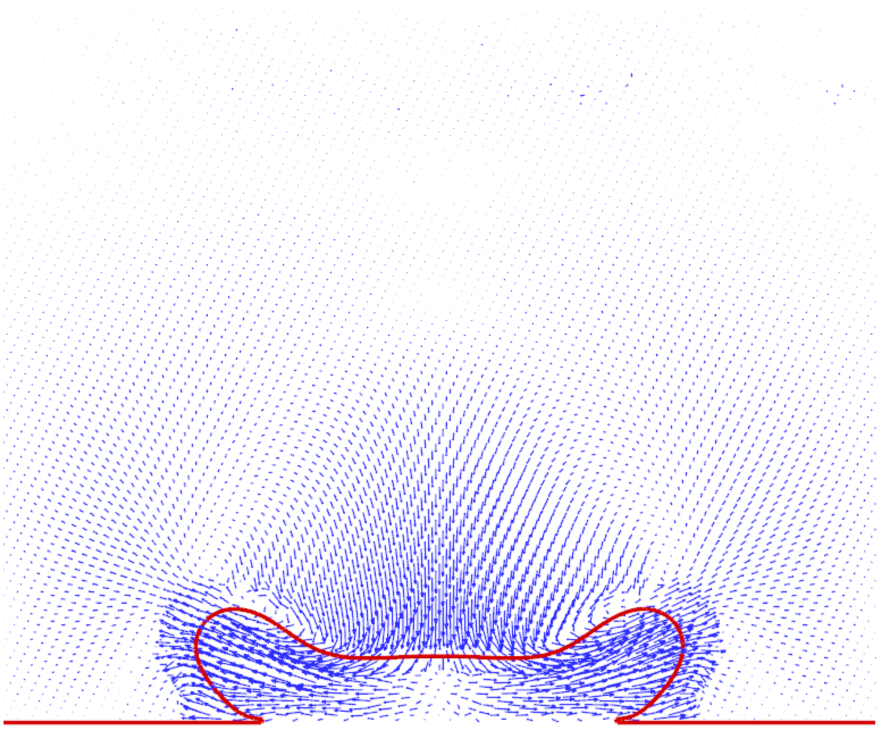

FIG. 2 . Complete-coalescence-rebound (CCR) regime. (a) Selected image sequence of impact and rebound behaviors of two droplets on a flat superhydrophobic surface with L =1.17 and We =35. The velocity fields are extracted along the mid y (b) and the mid$x$ (c) plane passing through the box. The normalized time is defined as$\tau =t\ /(\rho P\ _0{}^3/)^{1/2}$.

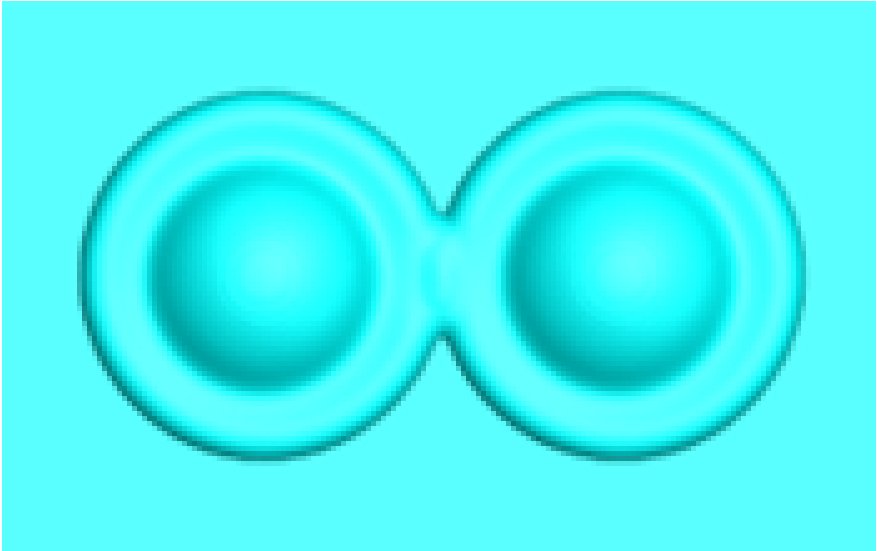

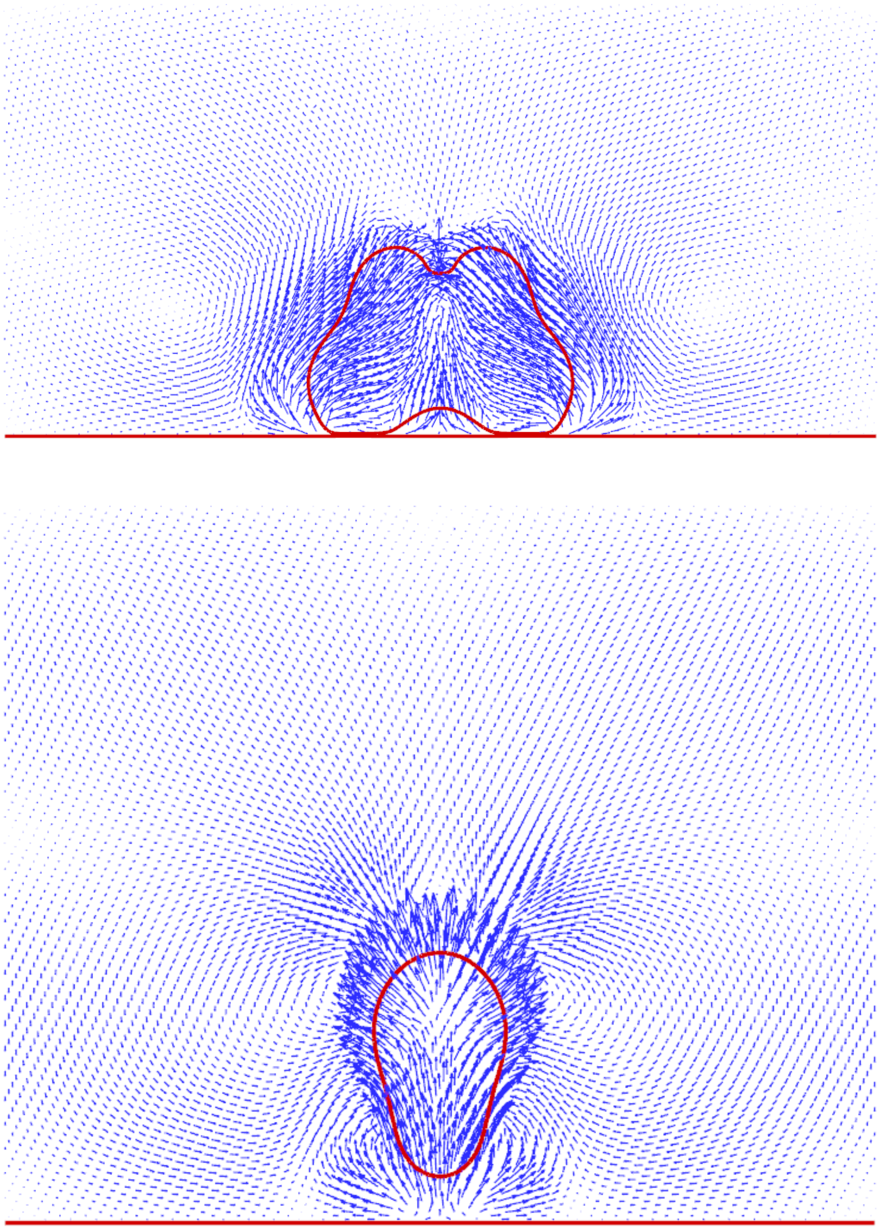

FIG. 3 . Partial-coalescence-rebound (PCR) regime. (a) Selected image sequence of impact and rebound behaviors of two droplets on a flat superhydrophobic surface with L =1.67 and We =35. The velocity fields are extracted along the mid y (b) and the mid$x$ (c) plane passing through the box. The normalized time is defined as$\tau = t\ /(\rho P\ _0{}^3/)^{1/2}$.

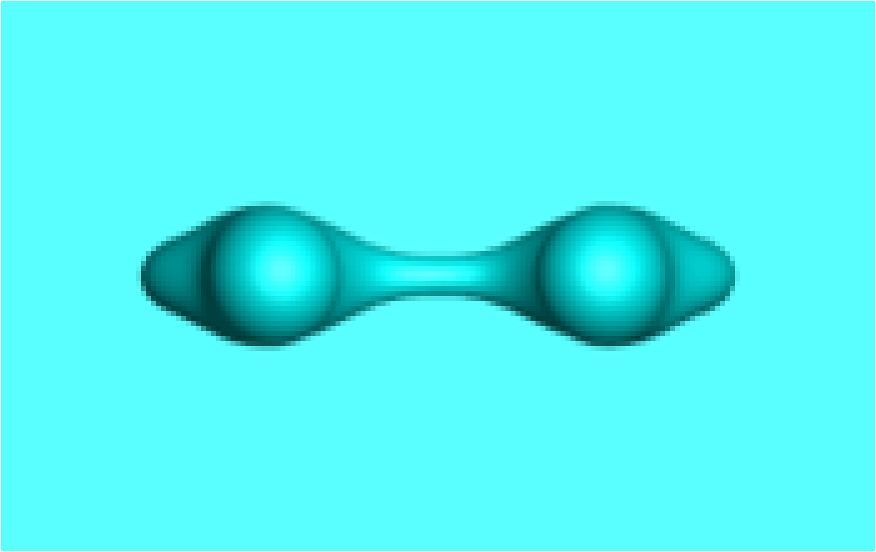

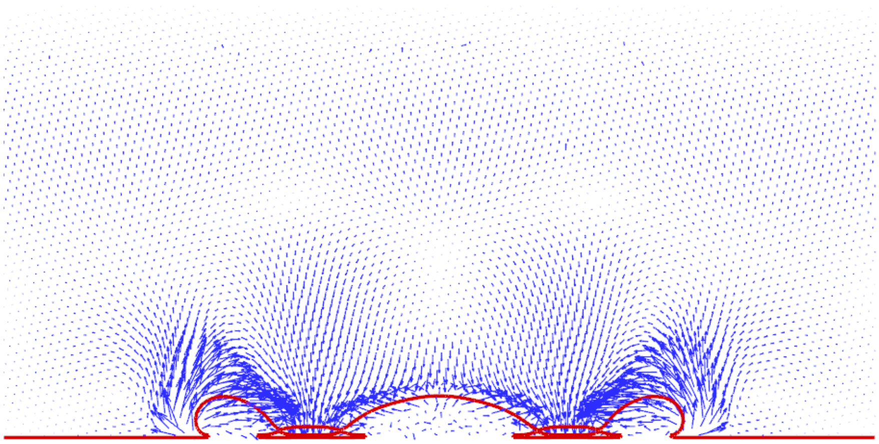

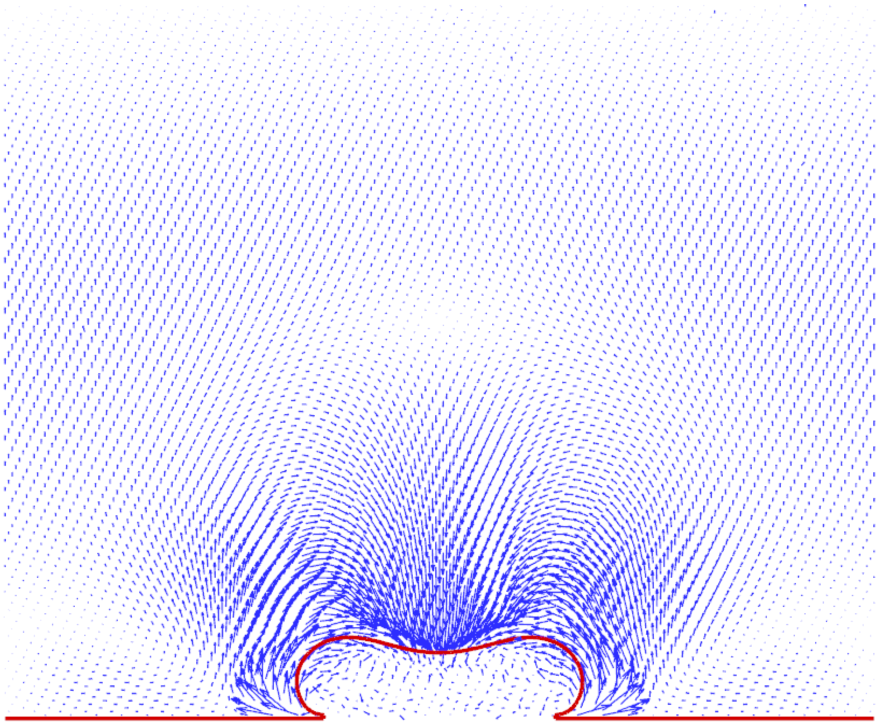

FIG. 4 . No-coalescence-rebound regime (NCR). (a) Selected image sequence of impact and rebound behaviors of two droplets on a flat superhydrophobic surface with L =2.00 and We =35. The velocity fields are extracted along the mid y (b) and the mid$x$ (c) plane passing through the box. The normalized time is defined as$\boldsymbol{\tau} = t\ /(\rho P\ {}_{0}{}^{3}/)^{1/2}$.

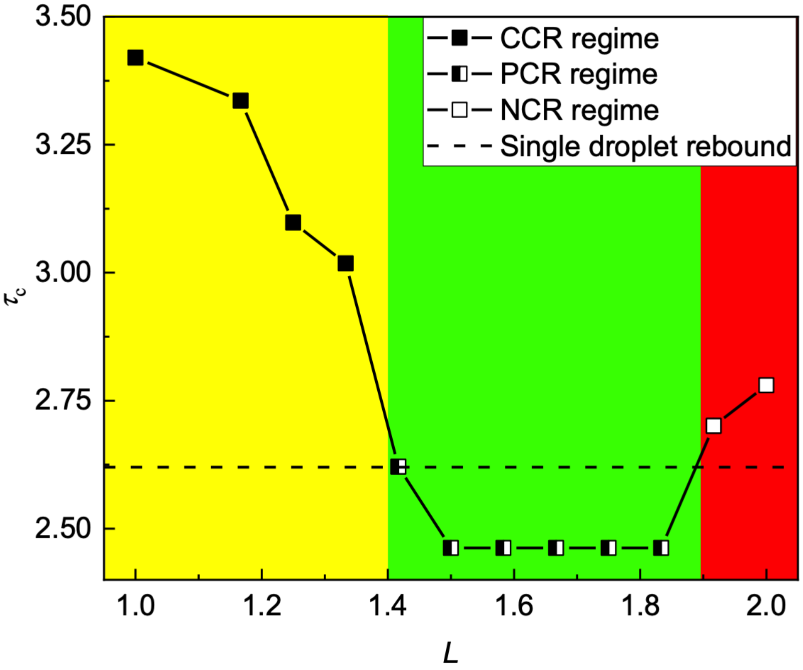

FIG. 5 . The normalized contact time as a function of the droplet distance at We =35.

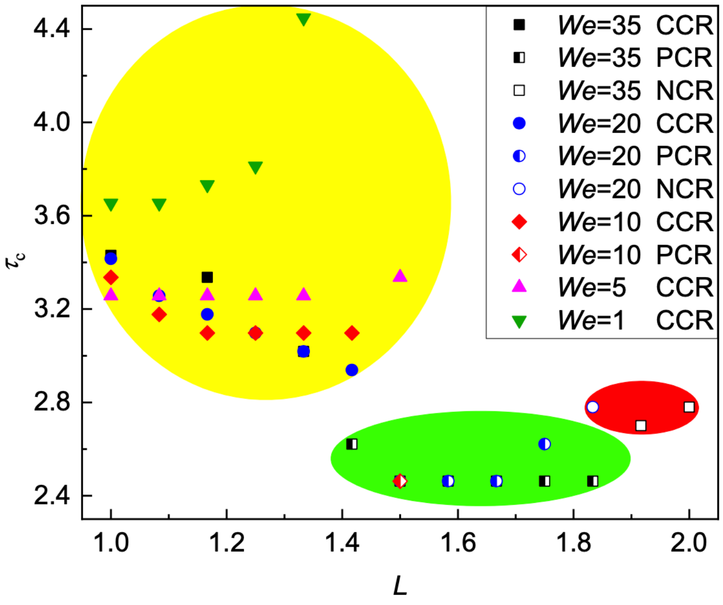

FIG. 6 . The normalized contact time as a function of the droplet distance at various Weber numbers.